Ocean Engineering 119 (2016) 165–180

Contents lists available at ScienceDirect

Ocean Engineering

journal homepage: www.elsevier.com/locate/oceaneng

Prediction of vertical responses of a container ship in abnormal waves

Suresh Rajendran, Nuno Fonseca, C. Guedes Soares *

Centre for Marine Technology and Ocean Engineering (CENTEC), Instituto Superior Técnico, Universidade de Lisboa, Portugal

ARTICLE INFO

Article history:
Received 22 October 2015
Received in revised form
25 January 2016
Accepted 20 March 2016
Available online 11 April 2016

Keywords:
Body nonlinear time domain code
Strip theory
Body nonlinear radiation/diffraction force
Memory function
Abnormal waves

ABSTRACT

A body-nonlinear time domain code based on strip theory is used to calculate the vertical ship responses of a containership in extreme sea conditions. The numerical method calculates the radiation forces based on Cummins formulation. A practical engineering approach is followed for calculation of the radiation/diffraction forces for instantaneous wetted surface of the hull. The Froude–Krylov and hydro static forces are also calculated for instantaneous wetted surface area of the hull. The numerical method calculates the vertical responses of a container ship in abnormal waves embedded in a real deterministic sea and the results are compared with the model test data. Results obtained from the numerical code that uses body-nonlinear hydrodynamic and hydrostatic forces are compared with results from another code that uses linear radiation/diffraction force and body-nonlinear Froude–Krylov and hydrostatic force. Time series of the vertical ship motion, vertical bending moment at the midship, and the relative motion at the bow are calculated and compared. Additionally, short term distribution of peaks of the vertical motion and bending moment, and the largest vertical bending moment peaks are analyzed. It is observed that the body nonlinear radiation/diffraction forces significantly improve prediction of the ship responses in extreme waves.

1. Introduction

Extreme sea conditions that involve waves with large amplitude to abnormal waves have always been an area of interest for naval architects, particularly, when their frequency of recent occurrence is reported to be higher than in the past. However, knowledge about behavior of sea going vessels in these extreme conditions is limited due to unavailability of real data and complexity involved with reproduction of such large deterministic wave profile in wave tank. Due to the same reason validation of numerical codes in extreme sea condition is not widely done.

Several methods varying from linear strip theory (Salvesen et al., 1970) to complex CFD (computational fluid dynamics) codes are available for prediction of ship responses in low to high seas. The ship responses are highly nonlinear in extreme seas and the nonlinearity mainly comes from two sources i.e. free surface and geometry of ship. The popularly known techniques to deal with the free surface nonlinearity are the weakly nonlinear formulations and the fully nonlinear numerical solutions. However, due to slender body assumption, it is generally believed that the geometrical nonlinearity associated with the hull is more important for estimation of the vertical response of ships. Sophisticated 3D panel methods, LAMP 2–4 (Lin et al. 2008), SWAN 2–4 (Kring et al. 1997), WISH (Kim et al. 2011), solves the disturbance potential for the exact body boundary condition and are accurate in prediction of the ship responses in small to moderate seas. The steady and unsteady potential are coupled more accurately. However, their main downfall is the heavy time consumption which questions their ability to use for calculation of extreme loads acting on a ship during its life cycle. The approximate method for calculation of the extreme loads is to fit a probabilistic model to several realizations of the short term distribution of loads (e.g. 3 h data) obtained in a few extreme sea states chosen from the scatter diagram. To the knowledge of the authors, it is not practical to use the aforementioned 3D panel methods for calculation of these extreme loads, at the least in the preliminary design stage.

The present work focus on a relatively simple and practical method, but still an accurate one, to estimate the ship responses to extreme sea states. The following paragraphs describe some of the background work that inspired the new developments presented herein. The time domain formulation of the equations of motion was presented by Cummins (1962) and widely used, later on, by various time domain codes based on strip theory. The time domain formulation replaced frequency dependent hydrodynamic coefficients with infinite frequency added mass, memory function and hydrodynamic restoring coefficients. Ogilvie (1964) formulated the hydrodynamic forces and moments in terms of linear potential functions used in Cummins' formulation. However, direct solution of these potential functions is very complicated; hence, the forces and moment were calculated by an analogy with the Fourier

* Corresponding author.
E-mail address: c.guedes.soares@centec.tecnico.ulisboa.pt (C. Guedes Soares).

http://dx.doi.org/10.1016/j.oceaneng.2016.03.043
0029-8018/

transform of frequency domain radiation forces, based on harmonic analysis and its pure physical rationality. Several variations of the nonlinear strip theory had been proposed, e.g., Xia et al. (1998), Wu and Moan (1996) and Fonseca and Guedes Soares (1998a, 1998b).

Xia et al. (1998) proposed a body nonlinear time domain method based on strip theory where the convolution integrals are sufficiently expressed through higher order differential equations for faster calculations. Wu and Moan (1996) proposed a nonlinear time domain method in which total response is decomposed into linear and nonlinear parts. The linear part is evaluated using appropriate linear potential-flow theory and the nonlinear part comes from convolution of the impulse response functions of linear ship-fluid system and the nonlinear hydrodynamic forces. Fonseca and Guedes Soares (1998) calculated the ship responses using a partially nonlinear time domain method based on strip theory. The radiation forces were calculated based on Cummins' formulation and Froude–Krylov and hydrostatic force were integrated up to the instantaneous water surface. They used the linear radiation and diffraction forces in the formulation by assuming that the nonlinear effects are dominated by the Froude–Krylov and hydrostatic forces. Mikami and Shimada (2006) calculated ship responses in large amplitude waves using a body nonlinear time domain code based on strip theory. They applied the first order Bernoulli pressure equation to the disturbance potential caused by an impulse. Based on relative motion concept, the radiation and diffraction forces were calculated. The memory functions were calculated using Fourier transforms of the hydrodynamic coefficients. Rajendran et al. (2011, 2012) calculated the vertical bending moment acting on a containership in abnormal waves using the aforementioned partially nonlinear code by Fonseca and Guedes Soares (1998). On comparison of the time series results from the same numerical method with model tests results in extreme seas, it was found that the partially body nonlinear method overestimated the sagging peaks. It was inferred later on that these discrepancies might be related to large variation in the hydrodynamic coefficients, which in turn results in large variation in the radiation/diffraction forces in extreme sea conditions. Therefore, the linear assumption for the radiation and diffraction forces might not be accurate for extreme sea states. Inaccurate calculation of the green water on deck effects was identified as another possible reason for the overestimation of extreme sagging peaks. Aforementioned strip theory based time domain methods takes account of the body nonlinearity partially or fully. However for faster calculation, most of them used approximations or variations of the Cummins formulation for calculation of the radiation forces, and relative motions concept for calculation of the diffraction forces. Rajendran et al. (2015a) proposed a body nonlinear method for calculation of the ship responses in extreme sea conditions. Geometrical dependency of the radiation/diffraction forces was taken into account through a simplified method but accurate enough for practical engineering applications. The radiation forces are represented by Cummins formulation and calculated for each time step for the exact wetted surface area under the incident wave profile and the diffraction forces are calculated from the potentials making use of Haskind relationship.

Responses of ships and offshore platforms to time series containing an abnormal wave have been studied, among others by Guedes Soares et al. (2006, 2008). These studies conducted a detailed time series comparison of the experimental and numerical vertical bending moment, along with the relative motion at bow and green water force on the deck of a Floating Production Storage and Offloading platform (FPSO) and the S-175 container ship, when encountering an abnormal wave (New Year Wave). The asymmetric nature of vertical bending moment time series was identified and usage of the nonlinear time domain code was discussed.

Clauss et al. (2005, 2009 and 2010) produced large abnormal waves in the wave basin of Technical University of Berlin, like the well-known New year wave, North Alwyn and 3 sisters, by special techniques that allowed superposition of higher order components to take account of their nonlinear interaction. This was achieved through a series of operations that started with identification of target parameters (e.g. for an abnormal wave $H_{target}=2H_s$, $T_{target}=T_P$, $\varsigma^a_{target}=0.6H_s$) from a JONSWAP spectrum and optimization of the random phase distribution for achievement of the aforementioned target parameter in time domain. This optimized signal serve as input signal for a wave generator and the waves generated in the physical wave tank are measured, however, it does not replicate the defined target parameter since nonlinear effects are insufficiently considered during the process. Accuracy of the waves in the tank is further increased through an automated experimental optimization process. Using this technique, it was possible to create a wide variety of extreme sea states like single abnormal waves or rogue waves embedded in real irregular sea state. The authors conducted tests with several types of ship models, including a container ship which is used as case study for the present study.

Reproduction of abnormal waves at an exact target location is a highly involved task. Using sophisticated techniques, here it is possible to compare numerical calculations with experimental results in such very large seas. In Rajendran et al. (2011), wave loads and vertical motion of a container ship in abnormal waves was calculated using a partially nonlinear code that used linear radiation/diffraction force and nonlinear Froude–Krylov and hydrostatic force. As mentioned before in the text, the method overestimated the extreme sagging moment peaks. In the present paper, wave induced structural loads and vertical motion of the same containership in abnormal waves are calculated using a modified code that uses the body nonlinear radiation/diffraction, Froude–Krylov and hydrostatic force and the improved results are compared with experimental results.

Hence forth the time domain (TD) code with the linear radiation force and nonlinear Froude–Krylov and hydrostatic force will be called 'partially body nonlinear time domain code' and the TD code with the nonlinear radiation/diffraction and Froude–Krylove/hydrostatic will be called 'fully body nonlinear TD code', even though there are many other elements of nonlinearity, e.g. slamming, higher order nonlinearities associated with the free surface and the body motion etc., that are not taken into account. Similarly, results from the partially body nonlinear method will be represented by symbol 'TD' and the results from the fully body nonlinear method will be represented by symbol 'TDNL' in the following figures.

2. Theory

Rajendran et al. (2015a) proposed and systematically validated a simplified body nonlinear method to calculate the ship responses in extreme sea conditions. The method calculates the hydrodynamic and hydrostatic forces for the exact wetted surface and is used in this paper to calculate the vertical responses of a containership in abnormal waves. The theoretical formulation behind the method is briefly described here again for the sake of completeness. A coordinate system fixed with respect to mean position of the ship is defined, $X=(x,y,z)$, with z in vertical upward direction and passing through center of gravity of the ship, x along longitudinal direction of the ship and pointing towards bow, and y perpendicular to the later and in the port direction. Origin is in the plane of undisturbed free surface. Considering a ship advancing in

waves and oscillating as an unrestrained rigid body, oscillatory motions will consist of three translations and three rotations. Although the theory is valid for arbitrary headings relative to waves, the present work was restricted to head waves, thus the oscillatory motions to be studied are surge and heave displacements and the pitch rotation.

Assuming inviscid flow the hydrodynamic problem is formulated in terms of potential flow theory. Further assuming small amplitudes of unsteady motions and incident waves, the velocity potential can be linearized. Substitution of velocity potential into linearized Bernoulli´s equation results in hydrodynamic pressure. Integration of oscillatory pressure terms over the wetted surface of the hull results in hydrodynamic forces associated with oscillatory ship motions in waves.

2.1. Radiation forces

2.1.1. Time domain radiation force

The radiation force in k-direction due to an oscillatory motion in the j-mode are expressed by means of infinite frequency added mass (A_{kj}^{∞}), memory function $(K_{kj}^{m})$and hydrodynamic restoring coefficients(C_{kj}^{m}).

$$A_{kj}^{\infty}\ddot{\xi}_j(t) + \int_{-\infty}^{t} K_{kj}^{m}(t-\tau)\dot{\xi}_j(\tau)d\tau + C_{kj}^{m}\xi_j(t)_5 = F_{kj}^{R}(t)\; k, j = 1, \ldots, 6 \quad (1)$$

The memory functions, K_{jk}^{m}, and radiation restoration coefficient, C_{jk}^{m},were calculated using the following equations:

$$K_{kj}^{m}(t) = \frac{2}{\pi}\int_0^{\infty}\left(B_{kj}(\omega)\cos\omega t\right)d\omega$$
$$C_{kj}^{m} = \omega^2\left[A_{kj}^{\infty} - A_{kj}(\omega)\right] - \omega\int_0^{\infty}\left(K_{kj}^{m}(\tau)\sin(\omega\tau)\right)d\; k, j = 1, \ldots, 6 \quad (2)$$

$A_{kj}(\omega)$ and $B_{kj}(\omega)$ represent the frequency dependent ship added masses and damping coefficients and the forward speed correction was applied through the strip theory method. For calculation of the zero speed coefficients, any 2D or 3D boundary element methods can be used.

In large amplitude waves, the ship's wetted surface area changed drastically and hence it should be taken into account, not only for calculation of Froude–Krylov and hydrostatic forces but also for radiation/diffraction force. Since it was our objective to include the body nonlinearity in the calculation of time domain radiation/diffraction forces, Eq. (2) along with infinite frequency added mass was to be updated at each instant of time before substituting in Eq. (1). Eq. (1) is still a linear formulation derived after application of linear radiation boundary condition. So the current formulation would be rather considered as a practical engineering approach for purpose of easy implementation and accurate results.

A new local coordinate system was defined for the each ship section as shown Fig. 1, where *OYZ* is the original coordinate system located at the mean water level and *oyz* is the new coordinate system. For each time step, the new coordinate system, *oyz*, is defined at the intersection between the incident wave profile, $Z=\zeta_I(X, Y, t)$, and the ship sections. The coordinate transformation between them could be written as

$x = X, y = Y, z(t)=Z-\zeta_I(t)$ and $\Phi(X, Y, Z, t)$ and $\phi(x, y, z, t)$, respectively, are the velocity potential defined in the original and new coordinate system.

The linear free surface condition can be written as

$$\frac{\partial^2\Phi}{\partial t^2} + g\frac{\partial\Phi}{\partial Z} = 0$$
$$\frac{\partial\Phi}{\partial t} = \frac{\partial\phi}{\partial t} + \frac{\partial\phi}{\partial z}\frac{\partial z}{\partial t} = \frac{\partial\phi}{\partial t} - \frac{\partial\phi}{\partial z}\dot{\zeta}_I$$
$$\frac{\partial^2\Phi}{\partial t^2} = \frac{\partial}{\partial t}\left(\frac{\partial\phi}{\partial t} - \frac{\partial\phi}{\partial z}\dot{\zeta}_I\right) + \frac{\partial z}{\partial t}\frac{\partial}{\partial z}\left(\frac{\partial\phi}{\partial t} - \frac{\partial\phi}{\partial z}\dot{\zeta}_I\right)$$
$$= \frac{\partial^2\phi}{\partial t^2} - 2\frac{\partial^2\phi}{\partial t\partial z}\dot{\zeta}_I - \frac{\partial\phi}{\partial z}\ddot{\zeta}_I + \frac{\partial^2\phi}{\partial z^2}\dot{\zeta}_I^2$$
$$\frac{\partial^2\phi}{\partial t^2} - 2\frac{\partial^2\phi}{\partial t\partial z}\dot{\zeta}_I - \frac{\partial\phi}{\partial z}\ddot{\zeta}_I + \frac{\partial^2\phi}{\partial z^2}\dot{\zeta}_I^2 + g\frac{\partial\Phi}{\partial z} = 0 \quad (3)$$

Based on weak scattering and small amplitude incident waves, the terms involving ζ_I are neglected and finally, the linear free surface condition is rewritten in the new coordinate system as

$$\frac{\partial^2\phi}{\partial t^2} + g\frac{\partial\Phi}{\partial z} = 0 \quad (4)$$

The linearized body boundary conditions do not change as they do not involve any time derivative, Chan et al. (2015). The boundary conditions are still linear; however the method is useful for calculation of the time dependent hydrodynamic forces. A practical engineering solution was followed in the present work in order to facilitate faster computation of the body nonlinear radiation/diffraction forces. The detailed explanation of the method can be found in Rajendran et al. (2015a) and are as the following.

1. Hydrodynamic coefficients were pre-calculated for each section for a number of drafts and stored in the database (added masses, damping coefficients and infinite frequency added mass) during the pre-processing stage.
2. During the time domain simulation, the 2D hydrodynamic coefficients stored in the data base were interpolated at each time instant for the exact draft of the sections.
3. The ship's global coefficients were computed at each time instant from the interpolated 2D coefficients and the forward speed corrections were introduced through the strip theory approach.
4. These coefficients were used to calculate the memory functions and the radiation restoring coefficients using Eq. (2). Similarly calculations were carried out for infinite frequency added masses and diffraction forces. They were substituted in the equation of motion and solved using the implicit trapezoidal method at each instant for motions, velocity and acceleration.

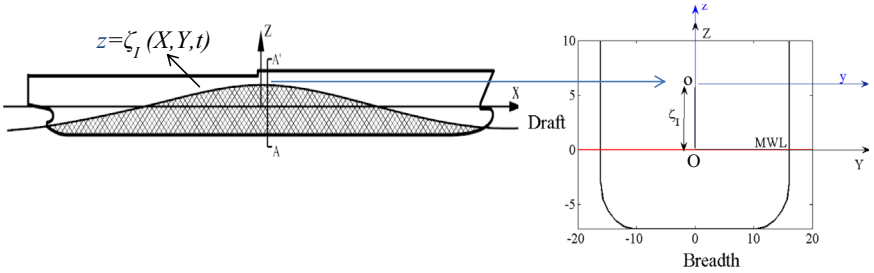

Fig. 1. Coordinate transformation between the original and new coordinate system.

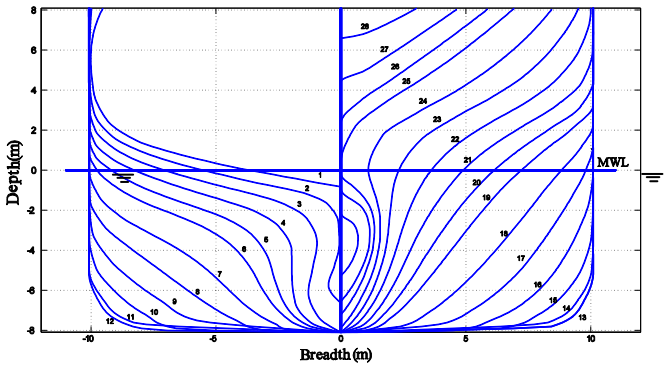

Fig. 2. Body plan for container ship.

2.2. Wave exciting and hydrostatic forces

2.2.1. Froude–Krylov force

The Froude–Krylov part is related to incident wave potential, and results from integration at each time step of associated pressure over wetted surface of the hull under the undisturbed wave profile. For regular waves traveling on negative x-direction, the Froude–Krylov force is given by:

$$F_k^I = g\rho \int_L \int_{Cx} \zeta^a n_k e^{ikx+kz} e^{i\omega t} dldx \quad j = 1, 3, 5 \tag{5}$$

where ζ^a is the incident wave amplitude and integration is over wetted cross section contour, C_x, under the incident wave elevation, n_k is the normal component in the respective direction of motion, ρ represents the density of the fluid, g is the gravity acceleration and k is the wave number, dl is the incremental length along the girth of ship section and 'z' is the instantaneous draft of the midpoint of a segment along the girth of a section. Pressure above the instantaneous mean water line is assumed to be hydrostatic.

The Froude–Krylov as well as the hydrostatic pressure was integrated over the whole wetted cross section contour, which included the deck when the wave was above the deck. Thus the effects of the water on deck were partially accounted, however the inertial effects were taken into account using the momentum conservation method proposed by Buchner (1995).

2.2.2. Diffraction force

Current study was restricted to head sea condition. Following Salvesen et al. (1970), but without neglecting the surge term, the diffraction force in head seas can be represented in terms of the sectional hydrodynamic coefficients.

For head seas, $\beta = 180°$, diffraction force and moment can be written as follow.

$$F_j^D(t) = \mathrm{Re}\Bigg\{ \rho\zeta_a\omega_0 e^{i(\omega_e t+\theta_k)} \int_L e^{ikx} \int_{Cx} e^{kz} \times \Bigg\{ \begin{matrix} (in_3 - n_1)\phi_j^0 - \\ \left[\frac{U}{i\omega_e}(in_3 - n_1)\phi_j^0 \right]_{j=5,6} \end{matrix} \Bigg\} dldx + \frac{\rho U\zeta_a}{i\omega_e} \int_{Cx} \omega_0 \Big[(in_3 - n_1) e^{ikx+kz} \Big] \phi_j^0 dl \Bigg\} \tag{6}$$

The strip theory separates the radiation force into speed dependent and independent part.

The speed independent part can be expressed in terms of sectional added mass (a_{kj}) and damping coefficients (b_{kj}) as given:

$$f_{kj}^{R2D} = -i\rho\omega_e \int_{Cx} n_k \phi_j^0 dl = \omega_e^2 a_{kj} - i\omega_e b_{kj} \tag{7}$$

Following the relationship given in (7), the surge diffraction force in head seas was calculated as given:

$$F_1^D(t) = \mathrm{Re}\Bigg[\zeta_a\omega_0 e^{i(\omega_e t+\theta_k)} \Bigg(-e^{kz}. \int_L e^{ikx}(i\omega_e a_{11} + b_{11}) dx - e^{ikx^A+kz^A} \omega_0 \frac{U}{i\omega_e}(i\omega_e a_{11}^A + b_{11}^A) \Bigg) \Bigg] \tag{8}$$

Similarly, heave diffraction force in time domain was calculated using

$$F_3^D(t) = \mathrm{Re}\Bigg[\zeta_a e^{i(\omega_e t+\theta_k)} \Bigg(-\omega_0 e^{kz}. \int_L e^{ikx}(\omega_e a_{33} - ib_{33}) dx - \zeta^a \omega_0 \frac{U}{i\omega_e} e^{ikx^A+kz^A}(\omega_e a_{33}^A - ib_{33}^A) \Bigg) \Bigg] \tag{9}$$

Pitch diffraction moment in time domain was calculated using

$$F_5^D(t) = \mathrm{Re}\Bigg[\zeta_a e^{i(\omega_e t+\theta_k)} \Bigg(\begin{matrix} \omega_0 e^{kz} e^{ikx} x. \int_L \left\{ \begin{matrix} (\omega_e a_{33} - ib_{33}) dx + \\ \frac{U}{i\omega} e^{ikx+kz}(\omega_e a_{33} - ib_{33}) \end{matrix} \right\} \\ + x^A \omega_0 \frac{U}{i\omega_e} e^{ikx*+kz}(\omega_e a_{33}^A - ib_{33}^A) \\ + \omega_0 e^{kz} \left\{ . \int_L (-iz(\omega_e a_{11} - ib_{11})) e^{ikx} dx \right\} \\ + \omega_0 \frac{U}{\omega_e} e^{ikx^A+kz^A}(z(-\omega_e a_{11}^A + ib_{11}^A)) \end{matrix} \Bigg) \Bigg] \tag{10}$$

where ζ_a is the incident wave amplitude, z is the vertical distance of the centroid of the underwater section from the newly defined frame of reference, $oxyz$, as shown in Fig. 1, ω_e is the encounter frequency between the ship and the waves, ω_0 is the wave frequency and θ_k is the phase angle of the input wave.

Body nonlinear diffraction force was calculated using (Eqs. (9) and 10) with the modified sectional added mass and damping coefficient. The added mass and the damping coefficients were calculated for the submerged section for each time step using the method discussed in Section 2.1.1.

2.3. Ship motions

2.3.1. Surge mode

Strip theory has several limitations, the hull 2-dimensionality being one of them. In fact, the hull is assumed to be slender so that the longitudinal component of the unit vector normal to the hull is considered null. The consequence is that there are no hydrodynamic forces related to the surge mode of motion. This limitation is overcome in the present method by including the surge mode in the equations of motion. Surge coefficients were calculated through a semi-empirical method proposed by Rajendran et al. (2015b). The basic idea was to calculate the sway hydrodynamic coefficient of an equivalent cross section with breadth and draft equal to length and draft of the ship, and sectional area coefficient equal to block coefficient of ship. Sway coefficients were calculated using multi parameter conformal mapping. However, these coefficients obtained through aforementioned method did not reflect any 3D hull effects. Final global surge coefficients were calculated by including 3D effects of surge motion through an empirical method. The linearized surge viscous damping was calculated from the derivative of frictional part of the hull resistance curve defined by ITTC 1957.

2.3.2. Equation of motion

An additional degree of freedom, surge, was introduced in the equations of motion related to the vertical ship responses. The final equations of motion could be written as given in (Eqs. (11)–13). The equation of motion was obtained by equating the hydrodynamic external forces to the mass internal forces. These equations were solved in the time domain by implicit trapezoidal method. For surge, heave and pitch, the equations of motions are as follow:

$$(M + A_{11}^{\infty})\ddot{\xi}_1(t) + \int_0^t K_{11}(t-\tau)\dot{\xi}_1(\tau)d\tau + C_{11}\xi_1(t) + (M.\,Z_{cg} + A_{15}^{\infty})\ddot{\xi}_5 + \int_0^t K_{15}(t-\tau)\dot{\xi}_5(\tau)d\tau + C_{15}\xi_5(t) = F_1^E(t) \quad (11)$$

$$(M + A_{33}^{\infty})\ddot{\xi}_3(t) + \int_0^t K_{33}(t-\tau)\dot{\xi}_3(\tau)d\tau + C_{33}\xi_3(t) + A_{35}^{\infty}\ddot{\xi}_5 + \int_0^t K_{35}(t-\tau)\dot{\xi}_5(\tau)d\tau + C_{35}\xi_5(t) + F_3^H(t) - Mg = F_3^E(t) + F_3^G(t) \quad (12)$$

$$(I_{55} + A_{55}^{\infty})\ddot{\xi}_5(t) + \int_0^t K_{55}(t-\tau)\dot{\xi}_5(\tau)d\tau + C_{55}\xi_5(t) + A_{53}^{\infty}\ddot{\xi}_3 + \int_0^t K_{53}(t-\tau)\dot{\xi}_3(\tau)d\tau + C_{53}\xi_3(t) + (M.\,Z_{cg} + A_{51}^{\infty})\ddot{\xi}_1 + \int_0^t K_{51}(t-\tau)\dot{\xi}_1(\tau)d\tau + C_{51}\xi_1(t) + F_5^H(t) = F_5^E(t) + F_5^G(t) \quad (13)$$

where ξ_1, ξ_3 and ξ_5 represent respectively the surge, heave and pitch motions and dots over the symbols represent differentiation with respect to time. M is the ship mass, g is the acceleration of gravity, Z_{cg} is the VCG of ship from MWL and I_{55} represent the ship inertia about the y-axis. The hydrostatic force and moment, F_3^H and F_5^H, are calculated at each time step by integration of the hydrostatic pressure over the wetted hull under the undisturbed wave profile. The exciting forces due to the incident waves, F_1^E, F_3^E and F_5^E, are decomposed into a diffraction part, F_1^D, F_3^D and F_5^D, and the well-known Froude–Krylov part, F_1^K, F_3^K and F_5^K. $F_3^G$and F_5^G represent the green water force and moment. A_{kj}^{∞} (j, k=1, 3, 5) is infinite frequency added masses are calculated the using multi-parameter conformal mapping technique, K_{kj} is memory function and C_{kj}^m is radiation restoration coefficient.

2.3.3. Relative motion

Difference between wave elevation and vertical displacement at a particular location of the ship gives the relative motion at that point. Relative motion was calculated using

$$\xi^r = \zeta^a - (\xi_3 - x\xi_5) \quad (14)$$

where ξ^r is the relative motion at a point ζ^a is the wave amplitude at the particular location, ξ_3 and ξ_5 are heave and pitch motions and x is the distance from COG of the ship to position where the relative motion is to be calculated.

Table 1
Main particulars of the container ship.

Length between perpendiculars [m], L_{pp}	117.6
Breadth [m], B_{WL}	20.2
Draught [m], D	8.1
Displacement [t]	12366.9
Block coefficient [dimensionless], C_B	0.65
LCG from aft [m], X_{cg}	59.02
VCG from baseline [m], Z_{cg}	7.35
Transversal metacentric height [m], GM_t	1.1
Scale of the model	1:70
Longitudinal inertia about center of gravity [kg m^2]	8.4648e+09

Table 2
Inertial properties of the containership model.

Description	Seg.1	Seg.2 (bow)	Trans.1	Trans.2	Trans.3
Weight, W (kg)	15.075	15.58	1.8	1.8	1.8
Longitudinal position of center of gravity from AP, Xg (m)	0.455	1.22	0.84	0.84	0.84
Lateral position of center of gravity, Yg (m)	0.000	0.000	0	0	0
Vertical position of center of gravity, Zg (m)	0.106	0.100	−0.01	0.187	0.187
Longitudinal inertia with respect to AP, Iyy (kg m^2)	3.4	23.46	1.27	1.27	1.27
Longitudinal inertia with respect to own center of gravity, Iyy (kg m^2)	0.446	0.429			

2.4. Wave loads

Wave induced global structural loads at a particular cross section were calculated from the difference between force/moment due to inertia and the sum of hydrodynamic and hydrostatic forces/moments at the part of the hull forward of that cross section.

$$M_k(t) = I_k(t) - R_k(t) - D_k(t) - K_k(t) - G_k(t) \qquad k = 1 \quad (15)$$

$$M_k(t) = I_k(t) - R_k(t) - D_k(t) - K_k(t) - H_k(t) - G_k(t) k = 3, 5 \quad (16)$$

where I_k is the force associated with the ship mass forward of the cross section under study. As assumed for calculation of the ship motions, radiation (R_k) and diffraction (D_k) hydrodynamic contributions for the loads are linear and body nonlinear, respectively, for partially and fully nonlinear TD code, and the Froude–Krylov (K_k) and hydrostatic (H_k) contributions are always body nonlinear and calculated over the "exact" hull wetted surface at each time step. $G_k$is the green water force.

The formulation for loads due to Froude–Krylov, diffraction and radiation forces remained the same as for motions, except the fact that the integration of forces should be carried out from the bow up to the cross section of interest. The convention for the loads was such that the sagging moment is negative and the hogging moment was positive. The exciting moment over the portion of the hull forward of the cross section under study was given by the diffraction and Froude–Krylov contributions, where the first was linear for partially nonlinear TD problem and body nonlinear for fully nonlinear TD problem and the second was body nonlinear for both. The hydrostatic contribution from each cross section was

Table 3
Description of the abnormal waves and the Froude number of the containership.

No	Type	Fn	H_s	T_p	H_{max}	AI
1	New Year Wave	0.0	11.91	16.3	24.5	2.06
2	New Year Wave	0.06	10.72	14.38	22.4	2.09
3	New Year Wave	0.12	12.92	13.32	26.2	2.03
4	North Alwyn	0.0	10.23	14.52	21.0	2.05
5	North Alwyn	0.06	9.21	12.31	18.94	2.06
6	North Alwyn	0.12	9.57	11.05	20.1	2.10
7	3 Sisters	0.0	10.22	8.95	18.7	2.09
8	3 Sisters	0.06	9.12	11.65	18.7	2.05
9	3 Sisters	0.12	8.51	10.44	14.96	1.76

Fn – Froude number, H_s – significant wave height, T_p – Peak wave period, H_{max} – maximum wave height, AI – Abnormality index.

given by the difference between the static equilibrium hydrostatic force and the actual hydrostatic force was calculated on the "exact" wetted surface.

2.5. Irregular waves

2.5.1. Wave elevation

Irregular sea states used for the numerical simulation were generated from the experimental wave times through Fourier transform. The time history of the undisturbed wave elevation was obtained by summing cosine wave components with the appropriate amplitudes ς_n^a, which corresponded to the defined wave amplitude spectrum. The waves were measured at midship of the ship and are transferred to COG of the ship using Eq. (17).

For waves traveling in the negative x-axis direction and represented on an earth fixed reference system, the wave elevation at a fixed point is given by:

$$\zeta(t, x) = \sum_{n=1}^{N} \zeta_n^a \cos(\omega_n t + k_n x + \varphi_n) \tag{17}$$

where ω_n are the wave frequencies in rad/s, k_n are the wave numbers and φ_n are phase angles of the experimental waves.

2.6. Rule bending moment

The IACS Common Rules (2009) provide the empirical formulae for the calculation of the design wave bending moment. The wave bending moment at the midship is given by the following formulae:

$$M_{W+} = 190CL^2BC_B \times 10^{-3} \text{ KN m for the hogging moment}$$
$$M_{W-} = -110CL^2B(C_B + 0.7) \times 10^{-3} \text{ KN m for the sagging moment} \tag{18}$$

where, $C = 10.75 - \left[\frac{300-L}{100}\right]^{1.5}$ for $90 \le L \le 300$, L=Length of the ship (L_{pp}) in meters, B=Molded breadth in meters, C_B=Block coefficient not less than 0.6.

3. Experimental setup and program

The container ship was tested in the seakeeping basin of the Ocean Engineering Division, Technical University Berlin (TUB). A computer controlled electrical driven wave generator, which can be used both as flap type and piston type, was used for the experiment. Table 1 presents the main particular of the ship and Table 2 gives the inertial property of the containership model and Fig.2 shows the body plan of the container ship.

The undisturbed incident wave elevation was measured with a wave gauge mounted on the towing arrangement moving with speeds of interest but without the model. Here the waves were measured in a moving frame of reference with the measurement carried out at the midship position. Heave and pitch motions were kept unrestrained by a suspension system connected with the model by thin elastic cross bar, which is mounted on the deck of the aft segment. These motions were measured by an optical tracking system installed on a carriage moving on roof mounted rails with same velocity of model. Clauss et al. (2009) present further details of the experimental setup for the container ship.

Abnormal waves were used to study the behavior of container ship in extreme seas. The waves in the tank were created by

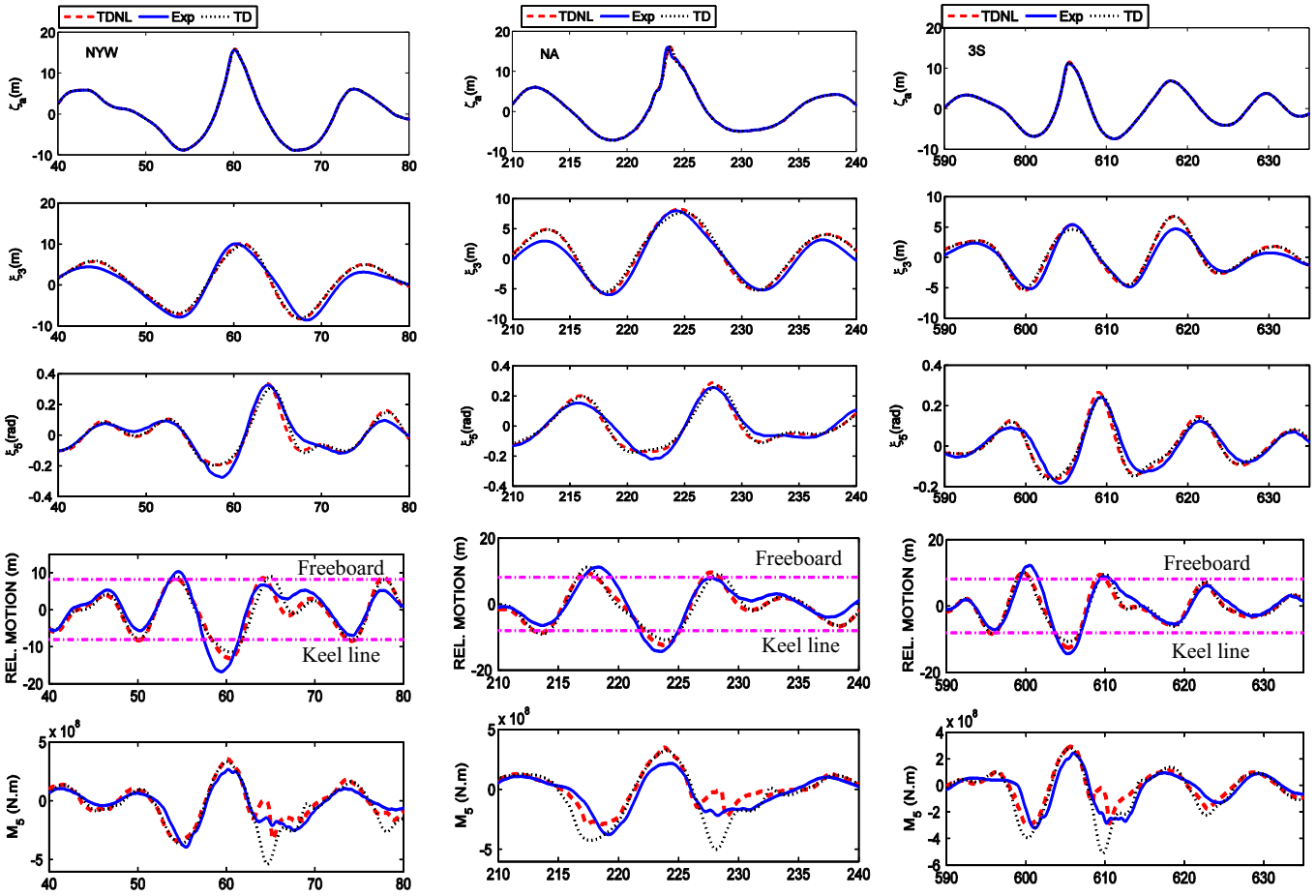

Fig. 3. Time series comparison of ship response in New Year Wave (left), North Alwyn (center) and three sisters (left) for 0 Fn.

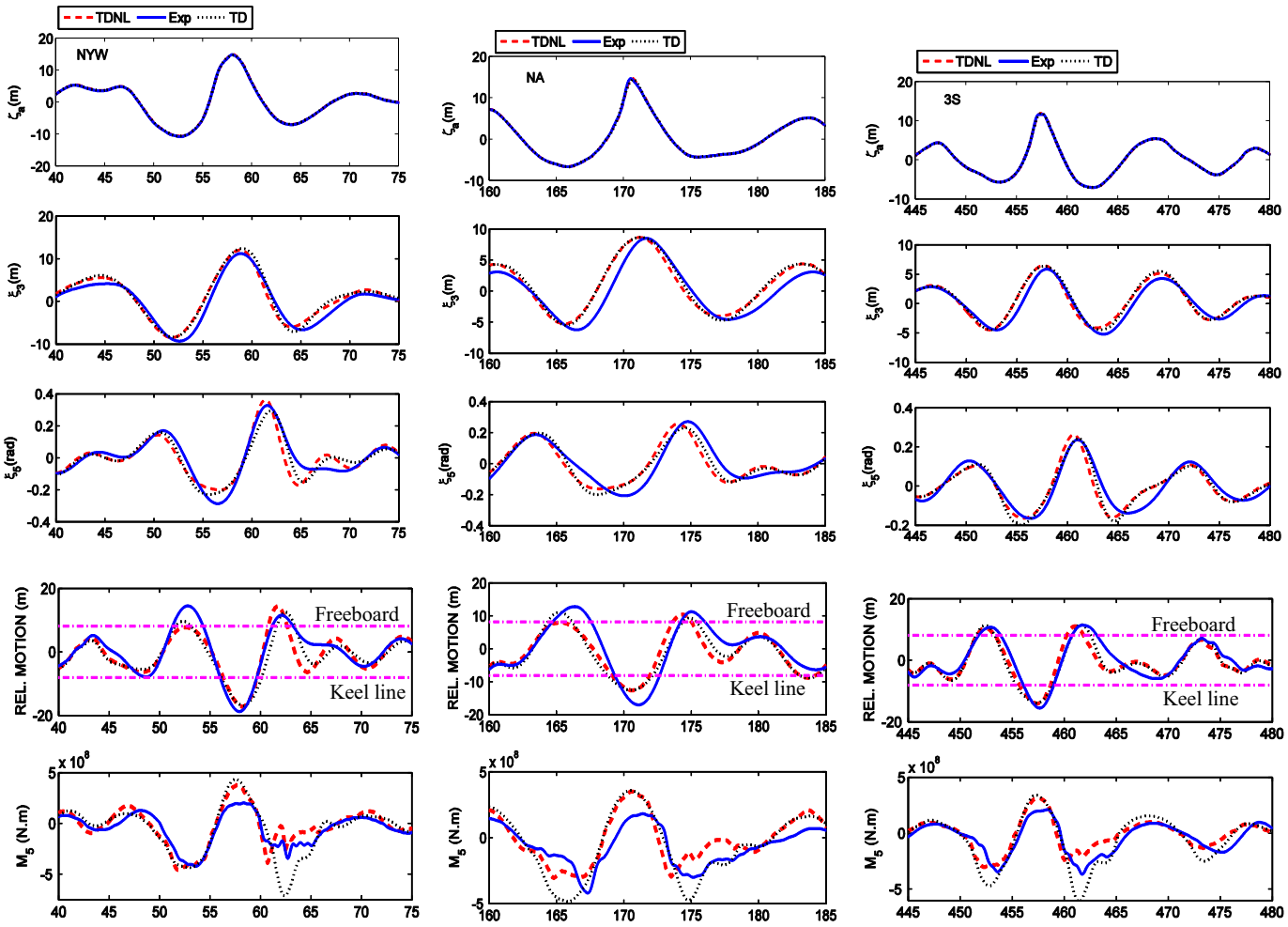

Fig. 4. Time series comparison of ship response in New Year Wave (left), North Alwyn (center) and three sisters (left) for 0.06 Fn.

superposing higher order components taking into account their nonlinear interaction (Clauss et al. 2010). Using this technique it was possible to create pre-defined single abnormal waves, like the well-known New Year Wave (Clauss and Schmittner, 2005), so as to study the effect of these abnormal waves on the ships. The container ship model consisted of two segments connected at Lpp/2 with three force transducers, two installed close to the deck level and other underneath the bottom of the model. The force transducers register the longitudinal forces during the model tests. Based on the measured forces and the given geometrical arrangement of the three force transducers, the resulting vertical wave bending moment and the longitudinal forces are obtained. On this basis, the superimposed vertical wave bending moment including the counteracting vertical bending moment caused by the longitudinal forces with respect to selected vertical levels is determined.

Table 3 gives a brief description of the abnormal waves and the Froude number of the containership used during this study. The test is conducted for three different Froude numbers in head seas. The New Year Wave, which was measured at the Draupner platform in North Sea in 1995, was recreated in the tank embedding in a dedicated irregular sea state. This giant wave produced in the wave tank had a maximum wave height of 24.5 m and a wave crest height of 15.75 m and the sea state is characterized by a significant wave height of 11.91 m ($H_{max}/H_s=2.06$). The significant wave height is calculated from the wave time series based on the zero up crossing. The ratio between the maximum wave height, $H_{max,}$ to the significant wave height, H_s, is referred as the abnormality index which is generally chosen by several authors as a reference to identify the abnormal waves. When the abnormality index of a wave is larger than 2, the wave is classified as an abnormal wave, Guedes Soares et al. (2003). Another abnormal wave measured at the North Alwyn platform in the North Sea and reported by Guedes Soares et al. (2003), was generated in the tank. This wave created in the tank had a maximum wave height of 22.4 m, with a maximum wave crest height of 16.1 m and the corresponding significant wave height is 10.72 m, with an abnormality index of $H_{max}/H_s=2.09$. The three sister waves are a group of three large waves traveling together. The largest wave produced in the lab had a maximum wave height of 18.7 m, and a wave crest and trough peak of 11.6 m and 7 m, respectively. The sea state is characterized with a significant wave height of 10.22 m and the largest wave has an abnormality index of 2.09.

4. Results

Ship responses from the two aforementioned numerical codes were compared with the experimental results. The partially nonlinear code took account of the body nonlinear Froude–Krylov and hydrostatic force, while the fully body nonlinear code considered the nonlinear radiation /diffraction forces additionally. Strictly speaking, the “fully nonlinear” expression in the context of seakeeping is used when the hydrodynamic boundary value problem is solved accounting for nonlinear free surface boundary condition and body exact boundary condition. The method used here is

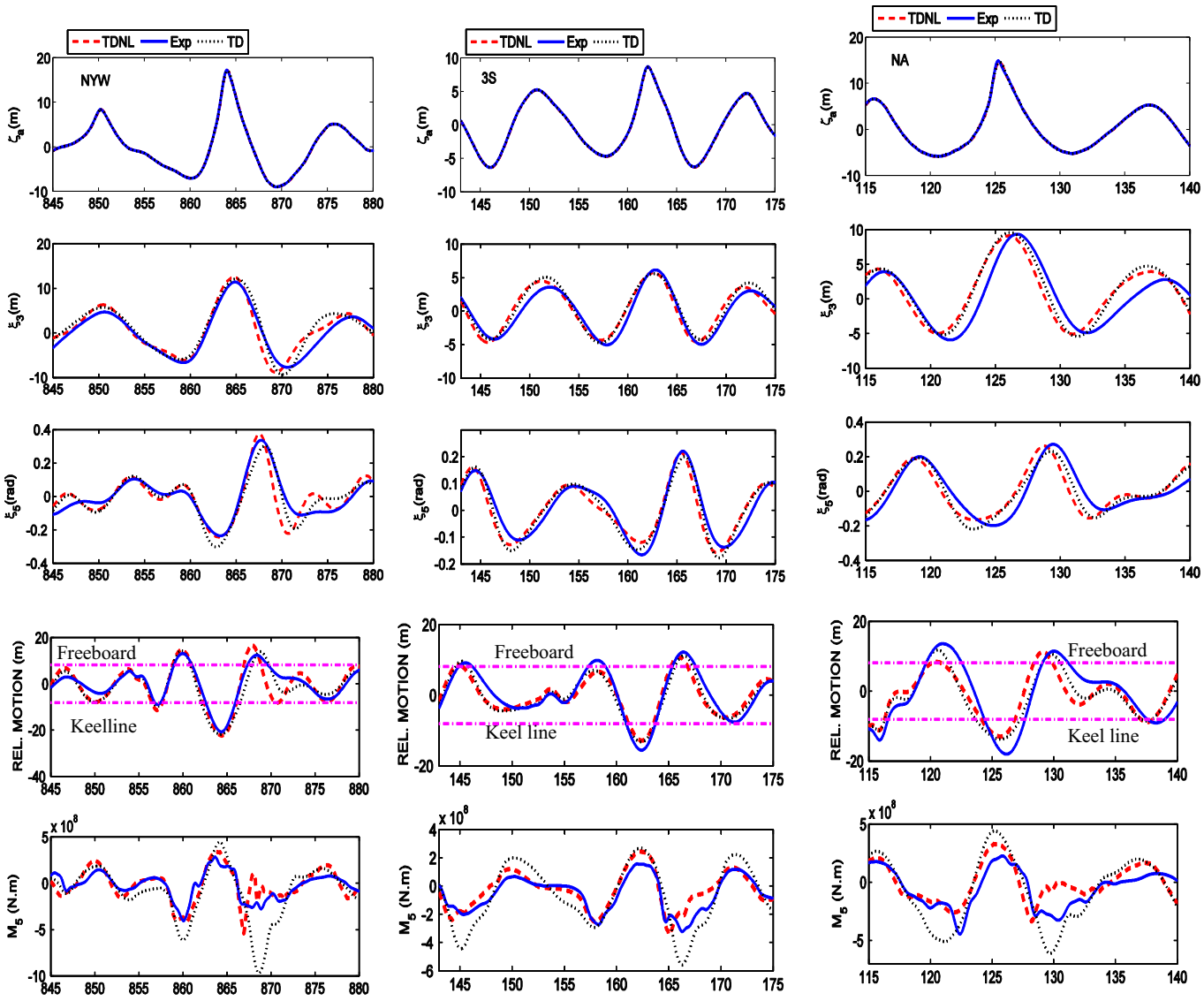

Fig. 5. Time series comparison of ship response in New Year Wave (left), North Alwyn (center) and three sisters (left) for 0.12Fn.

simpler, since the nonlinear effects were represented by a practical engineering approach. However the expression "fully body nonlinear" is used to highlight the characteristics that all forces in the equations of motion were body nonlinear.

Time series of the ship responses are compared in the first Section. The ship responses included the vertical motions, relative motion at the forward perpendicular (58.8 m forward of the midship) and the vertical bending moment at midship. The time series comparison of the ship response was carried out separately for different Froude numbers, i.e. for 0, 0.06 and 0.12 Froude numbers. This was followed by the comparison of the probability of exceedance of the peaks of the numerical and the experimental ship responses in three different irregular seas. Each irregular sea included an abnormal wave. Finally, the first and second largest peaks of the vertical bending moment from the two numerical methods were compared with the experimental results.

4.1. Vertical ship motions and bending moments

4.1.1. Time series comparison of the responses of the stationary ship

The incoming abnormal waves and the associated vertical ship responses of the container ship in the New Year, North Alwyn and 3 Sisters waves are shown in Fig. 3. The numerical and the experimental results are compared with each other. The thick bold line denotes the experimental results and the dashed and dotted lines, respectively, show the numerical results from the fully body nonlinear and partially body nonlinear time domain methods. The ship responses were measured and calculated in head seas for zero Froude number. The abnormal waves were embedded in a real deterministic sea. The incoming wave elevation was measured at amidship (during the calibration run), which also serves as the input for the numerical calculation. Therefore, the numerical and the experimental incoming waves at amidship coincided with each other as shown in the plot. The harmonics of the measured wave were obtained by means of Fourier analysis and the wave elevation at amidship was recreated in the numerical method using Eq. (17). However, the numerical method spatially propagated these waves along the length of the ship using linear dispersion relationship. Therefore, the numerical incoming waves might be different from the real waves at longitudinal positions away from the midship. The analyzed ship responses included the absolute vertical motions, i.e. heave and pitch motions, the relative motion at the bow and the vertical bending moment at amidship. The relative motion at the bow was calculated using Eq. (14). Two horizontal lines in the relative motion plot denote the height of the freeboard and the keel line.

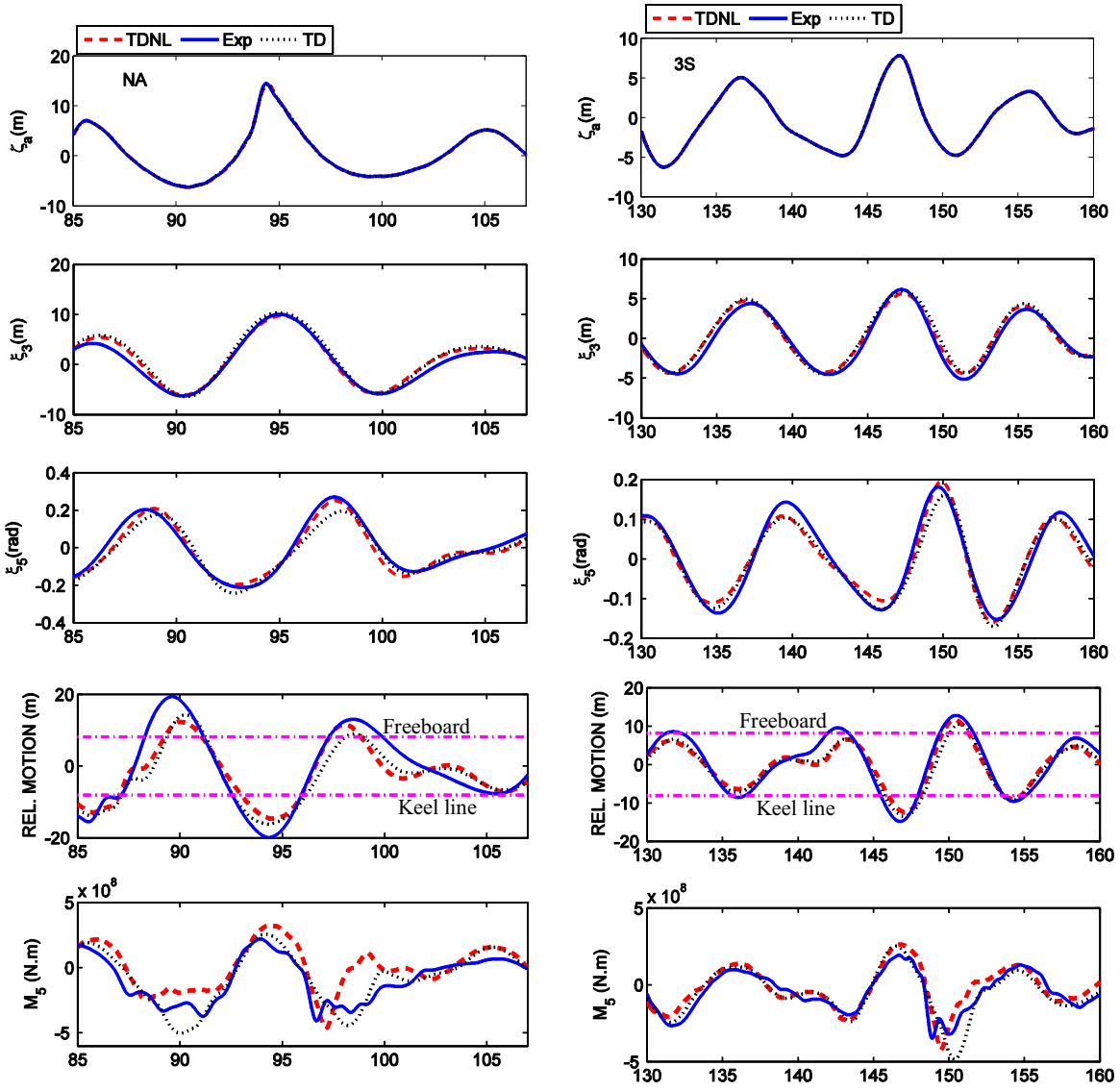

Fig. 6. Time series comparison of ship response North Alwyn (left) and three sisters (right) for 0.18Fn.

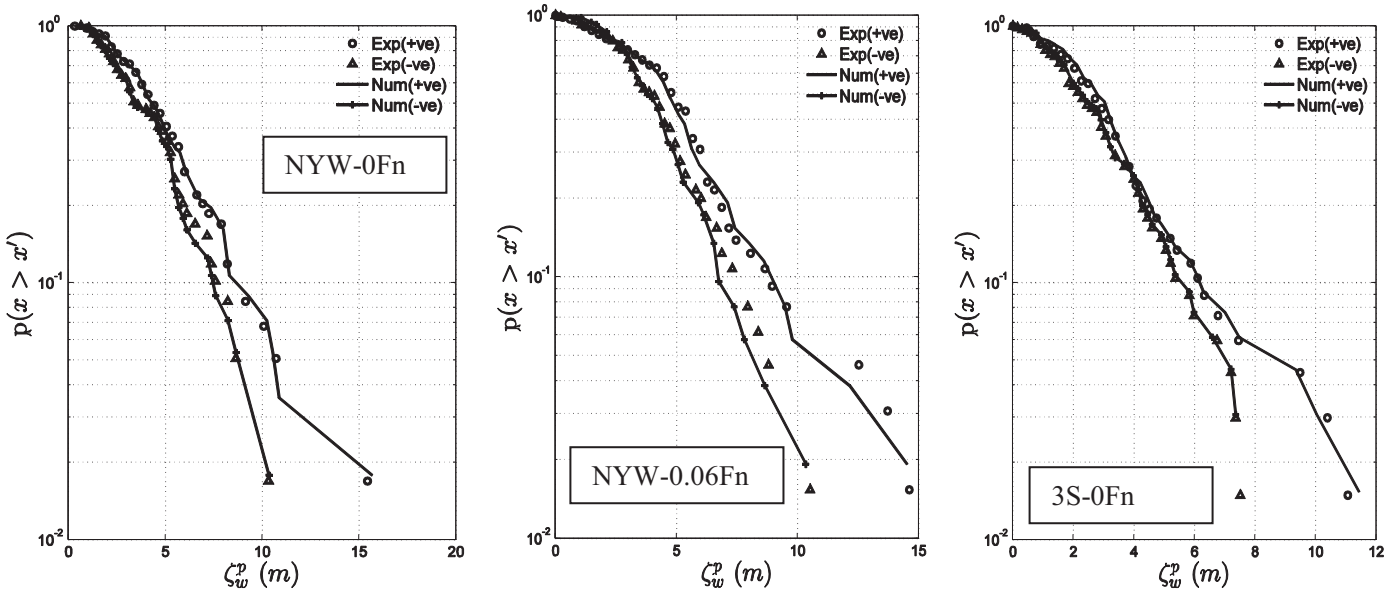

Fig. 7. Comparison of probability of exceedence of the numerical and the experimental incoming wave peaks. The abnormal waves are embedded in these sea states.

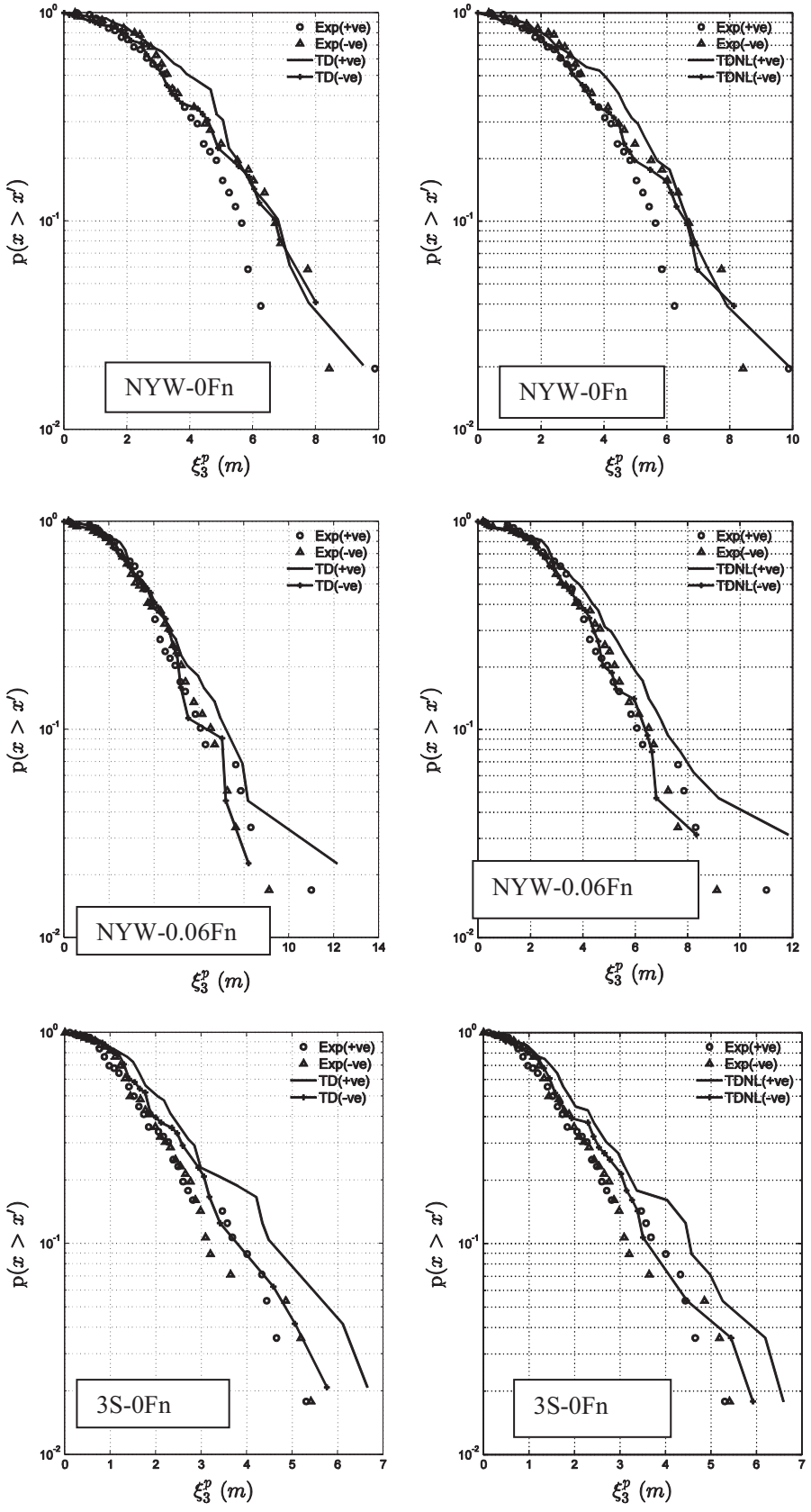

Fig. 8. Comparison of probability of exceedence of the numerical and the experimental heave peaks in irregular seas embedded with the abnormal waves. The plots on the left compare the experimental results with the results from the partially bodynonlinear methods. The plots on the right shows the comparison of the experimental results with the fully bodynonlinear method.

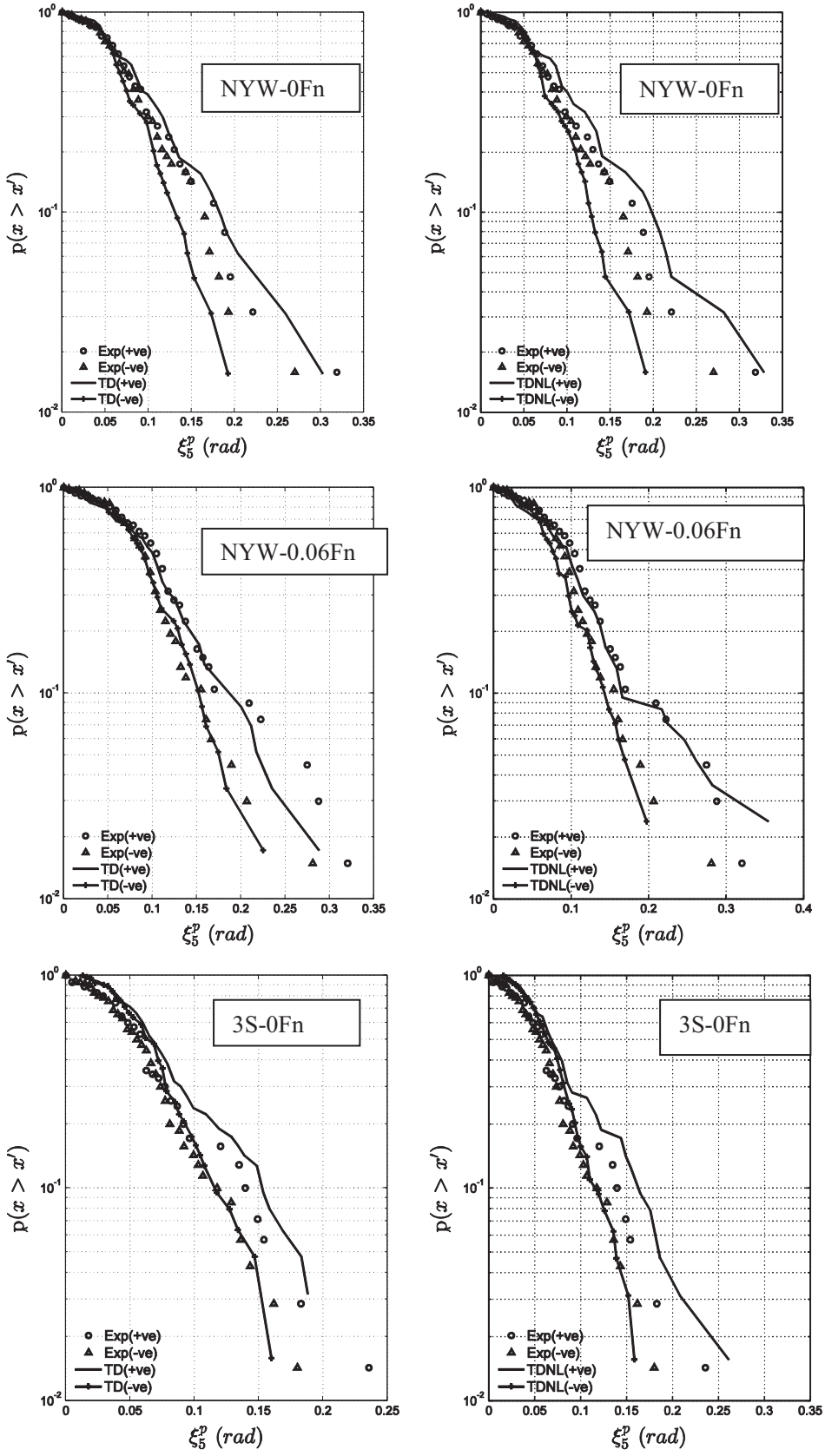

Fig. 9. Comparison of probability of exceedence of the numerical and the experimental pitch peaks in irregular seas embedded with the abnormal waves. The plots on the left compare the experimental results with the results from the partially bodynonlinear methods. The plots on the right shows the comparison of the experimental results with the fully bodynonlinear method.

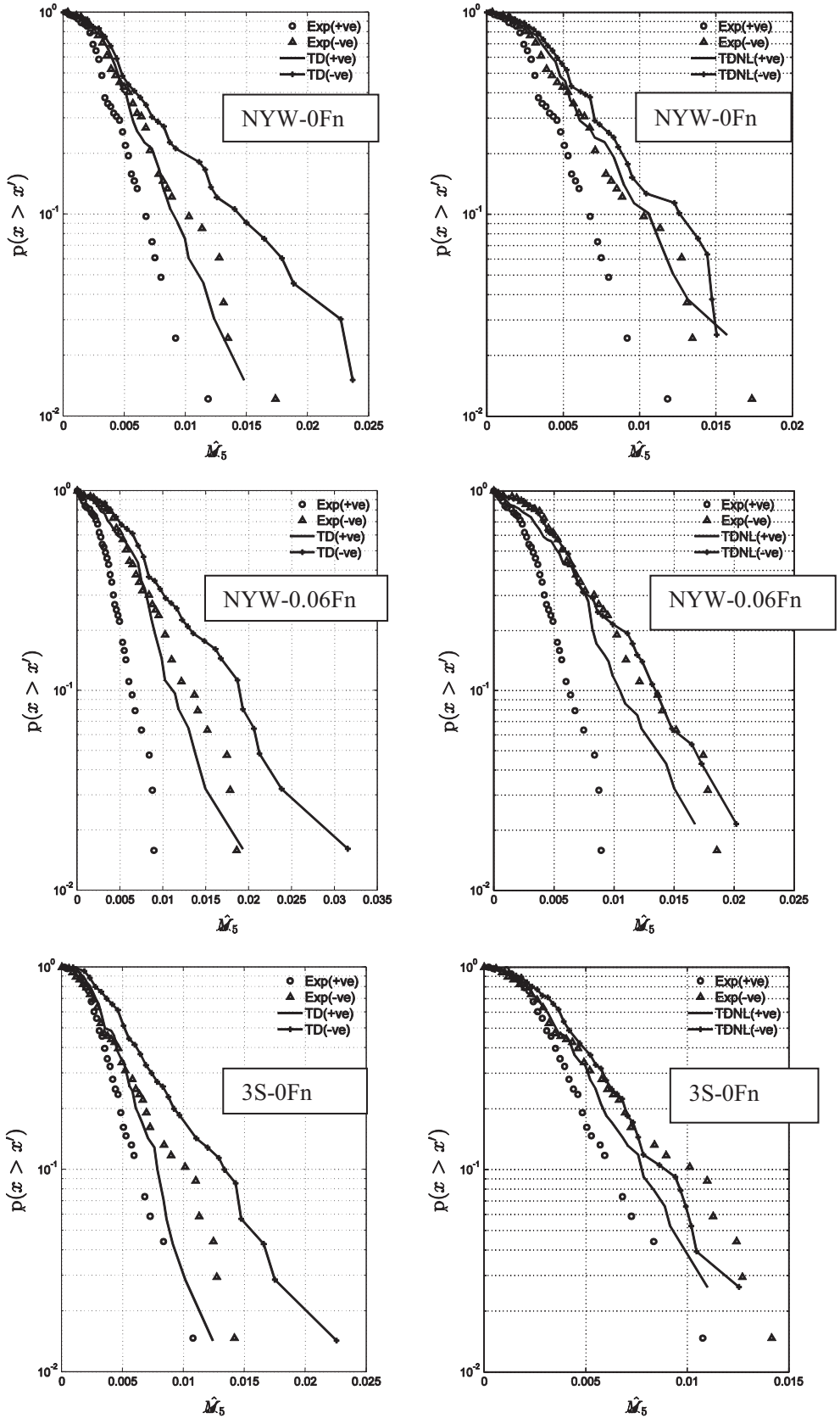

Fig. 10. Comparison of probability of exceedence of the numerical and the experimental vertical bending moment peaks in irregular seas embedded with the abnormal waves (70 cycles) The plots on the left compare the experimental results with the results from the partially bodynonlinear methods. The plots on the right shows the comparison of the experimental results with the fully bodynonlinear method.

Table 4
Percentage of error in the calculation of first and second largest vertical bending moments between nonlinear code (TDNL) and experimental results (−ve value indicate smaller numerical value).

Description	1st largest sagging peak	2nd largest sagging peak
New Year Wave (0 Fn)	10%	−16%
North Alwyn (0 Fn)	−3	−5
Three sisters (0 Fn)	−4	−12
New Year Wave (0.06 Fn)	−9	19
North Alwyn (0.06 Fn)	15	9
Three sisters (0.06 Fn)	20	2
New Year Wave (0.12 Fn)	−19	13
North Alwyn (0.12 Fn)	−7	17
Three sisters (0.12 Fn)	−24	−19

The crest and the adjacent troughs of the New Year wave (NYW) are shown in Fig. 3 (left graphs). The height of the crest peak was 15.75 m and the trough peak was 8.7 m.The wave length estimated between the two adjacent troughs was 263.8 m, which is 2.24 times the length of the ship. The center plot in Fig. 3 shows the ship responses in the North Alwyn (NA) abnormal wave. The height of the peak of the wave crest was 16.1 m and the trough peak was 7 m. The estimated wave length between the adjacent troughs was 189 m, which is 1.6 times the length of the ship. The right plots in Fig. 3 show the ship responses in 3 sister waves (3 S), which was a group of 3 consecutive large waves, with a large middle wave followed and preceded by smaller waves. The height of the largest wave crest peak was 11.6 m and the trough peak was 7 m. This wave was followed by a 14 m wave and preceded by a 10 m wave. The length of the wave measured between the trough peaks adjacent to the largest wave was 156 m which is 1.32 times the length of the ship.

In general, the heave motions associated with the abnormal waves were in phase with the incident wave motion at the center of gravity of the ship (0.22 m forward of midship section). The numerical heave responses were in good agreement with each other which showed that the body nonlinear radiation/diffraction forces did not have any significant effect on the heave responses when the ship encountered the abnormal wave. Similarly, the body nonlinear hydrodynamic forces slightly affected the pitch motion. The ship emergence was slightly over estimated and the bow emergence was underestimated by the numerical methods. The exact reason behind such behavior is not understood. However, it is presumed that the slight discrepancy between the results could be due to the following reasons. 1) Due to the 2D assumption, the strip theory has a tendency of the strip theory to overestimate the hydrodynamic coefficients, particularly for zero speed case. This generally led to underestimation of the vertical motions by the strip theory. 2) Viscosity, which depends on the heave and pitch velocity, could play a significant role in the extreme ship responses in extreme seas. Viscosity can result in flow separation, particularly below the flat bottom, when the ship emerges (+ve heave motion) or when the bow emerges (−ve pitch motion) and try to dampen the ship responses leading to lower ship motions in the wave basin. Viscous damping was not considered in the potential code. 3) The experimental wave elevation was used in the numerical method, which facilitated the exact calculation of the hydrostatic forces. However, the Froude–Krylov pressure was calculated based on the linear theory and the pressure distribution under the crest and trough were symmetrically distributed. For the experimental waves which were highly nonlinear, the Froude–Krylov pressure under the larger crests and shallows troughs were asymmetrically distributed with larger pressure under the crest. The numerical methods did not take into account the higher order nonlinearity associated with the free surface waves, therefore depending on the wave profile along the length of the ship, the linear waves might result in under or overestimation of the exciting forces.

The vertical bending moment at the midship largely depends on the relative motion at the bow. The body nonlinearity had only little effect on the vertical motions. This was mainly due to the major role played by the long parallel middle body in the ship motion for which the changes in the added mass and damping coefficient for a range of draft were not significant as it was for the aft and fore sections of the ship. However, the body nonlinearity played an important role in the calculation of the bending moment at the midship because of the significant contribution from the geometrical nonlinearity (pronounced bow flare) of the bow section. The fully body nonlinear method was able to give good estimation of the vertical bending moment whenever the wetted surface area in the numerical model agreed with the experimental results as depicted in the relative motion plot. The partial nonlinear method overestimated the sagging peaks because of the underestimation of the radiation forces which resulted from the lower submersion (radiations forces calculated only up to the mean draft) of the bow region than the real scenario. Due to the large bow flare angle, larger submersion of the bow resulted in larger potential damping due to the increase in the breadth of the bow sections. In the fully body nonlinear method, this increase in the potential damping value resulted in reduced bending moment.

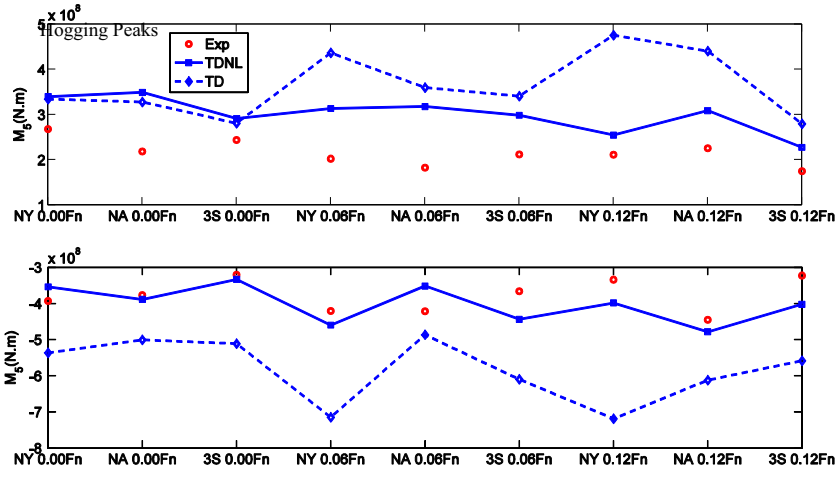

*NY-New Year wave, NA-North Alwyn, 3S-3 Sisters, Fn-Froude number

Fig. 11. Comparison of First largest hogging and sagging peaks.

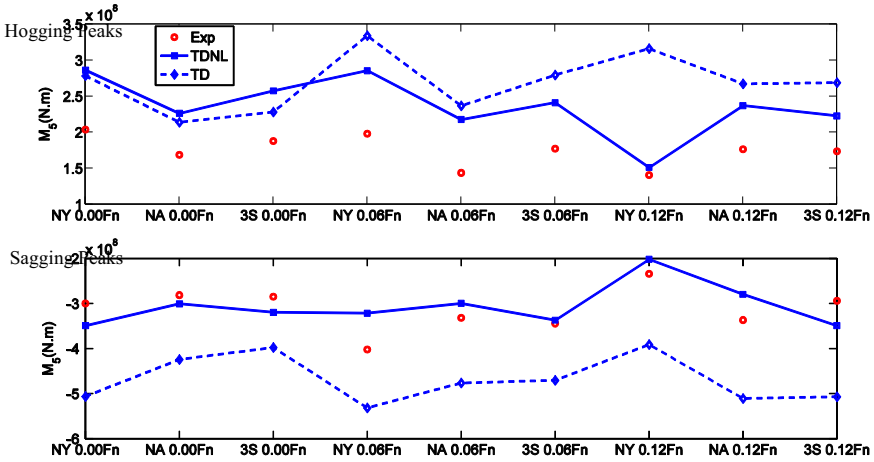

*NY-New Year wave, NA-North Alwyn, 3S-3 Sisters, Fn-Froude number

Fig. 12. Comparison of second largest vertical bending moment.

4.1.2. Time series comparison of the responses of the ship underway

Similar to the discussion held in Section 4.1.1, the calculated and the measured wave elevation and the ship responses in abnormal waves are compared in Figs. 4–6 for which the ship moves with a Froude number of 0.06, 0.12 and 0.18, respectively, in head seas. The symbols used in the plot remains the same as mentioned in the previous section. Regarding the heave peaks, the numerical results were in good agreement with the experiment. The positive pitch motion peaks from the numerical results compared well with the measured responses. However, slight discrepancies were observed while predicting the bow up (negative pitch) condition as observed for the zero speed case. The underestimation of the forward speed effects by the strip theory, particularly for the heave on pitch coupling coefficients could also play an important role here. Apart from that, the steady bow waves and the dynamic swell up where the bow pushes the water higher than what was measured could alter the incident wave elevation. The radiated and diffracted waves could also distort the wave condition around the midship which added to the complexity. The shipping of green water and slamming is observed in both the numerical and the experimental results. In general, the green water height is under predicted by the numerical results and the height of fall during slamming measured during the experiment was larger than the numerical results. Regarding the vertical bending moment, the fully body nonlinear results were in good agreement with the experimental results, particularly for the sagging peaks, while the partially nonlinear predictions overestimated the same sagging peaks and the hogging peaks were slightly overestimated by the numerical methods.

4.1.3. Probability of exceedance

Probabilities of exceedance of the peaks of the numerical and the experimental waves and responses were compared. In order to obtain a reliable data for the short term distribution of the wave and response peaks, only those sea states with a number of wave cycles larger than 60 were considered for the analysis. This provided a fair insight into the behavior of the ship in these irregular seas, even though a larger number of wave cycles would reduce the statistical uncertainty. Therefore, short term distribution of the ship responses in three irregular sea states was presented. The abnormal waves were embedded in these irregular, therefore the abnormal waves were used to name the sea states. The following cases were considered: 1) New Year Wave (NYW) encountering stationary ship; 2) New Year Wave encountering the ship with 0.06 Froude number; 3) Three Sister (3 S) wave encountering a stationary ship.

Fig. 7 compares the peaks of the measured waves at the midship and the numerical incoming waves at the center of gravity of the ship. The center of gravity of the ship was slightly offset from the midship, i.e. 0.4 m forward of the midship.

Fig. 8 compares the probability of exceedance of the numerical and the experimental heave peaks in three irregular sea states mentioned above. The numerical results included the results from the partially body nonlinear method, which is presented on the figure left side, and the results from the fully body nonlinear method are presented on the right side. Circles and triangles are used to represent the experimental positive and negative peaks. Solid lines and the line with plus mark are used to denote the numerical positive and negative peaks. The experimental heave peaks were symmetrically distributed up to 4 m, beyond which the distribution becomes asymmetric. For the analyzed cases, the numerical negative heave peaks were in good agreement with the measured heave responses, i.e. the ship submergence was well predicted by the numerical methods. However, the ship emergence (positive heave peaks) were overestimated by both numerical codes. The time series comparison carried out in Section 4.1.1 showed similar results and the discussion had been held. There was no distinguishable difference between the numerical results from the two methods.

Short term distribution of the peaks of the pitch motion in irregular seas is presented in Fig. 9. Asymmetry in the distribution of the experimental peaks is observed beyond 0.1 rad – the magnitude of positive peaks (bow down) tends to be larger than the negative peaks. There was a good agreement between the numerical and the experimental results. The numerical method was able to give a good estimation of the emergence and submergence of the bow. The fully body nonlinear method improved the calculation of the pitch motion, particularly when the ship moved with 0.06 Froude number in irregular sea with New Year Wave.

The probability of exceedance of the numerical and the experimental sagging and hogging bending moment peaks are compared in Fig. 10. The vertical bending moment is made non-dimensional with $\rho g L_{pp}^2 BT$, where L_{pp} is the length between perpendiculars, B is the breadth of the ship, ρ is the density of water, g is the acceleration due to gravity and T is the draft of the ship. For the analyzed three cases, the largest experimental sagging peak never went beyond a non-dimensional value of 0.02. The distribution of the experimental peaks was highly asymmetric with larger sagging values. The partial body nonlinear method largely

overestimated the sagging peaks while the sagging peaks from the fully body nonlinear method was in good agreement with the experimental results. This showed the necessity to take into account the body nonlinear radiation and diffraction forces for the calculation of the ship response in extreme seas, particularly for ships with large bow flare.

Clauss et al. (2010) conducted model tests on a Ro–Ro vessel and a bulk carrier ship in regular waves with varying steepness (from low to high) and compared the experimental sagging and hogging peaks with RAOs obtained through transient wave technique. Asymmetric characteristics of vertical bending moment was observed for Ro–Ro vessel in waves with large steepness, however, the bending moment acting on the bulk carrier was more or less symmetric for all wave steepness. This was mainly attributed to the large bow flare of Ro–Ro vessel which affects the nonlinearity of responses. Similarly, Rajendran et al. (2013) calculated the vertical bending moment acting on a cruise vessel in extreme sea condition. The cruise vessel also possessed large bow flare above the mean water level. The partially body nonlinear method overestimated the sagging peaks, while the fully body nonlinear method gave a good estimation of the peaks of the vertical bending moment at the midship. It was stated that "damping coefficient values of the bow sections significantly increase as the draft increase, because of increase in breadth. For the wall sided midship sections, damping of the sections increases as draft decreases since for the same breadth, deeper sections possess less damping. Deeper submersion at bow and lower submersion at midship sections, which correspond to sagging moment, result in larger potential damping than calculated at the mean draft due to aforementioned reasons. Neglecting this increased damping may be the reason that results in overestimation of sagging peak for the partially nonlinear time domain code". Large immersion of the bows with pronounced bow flare angle significantly changed the wetted surface area and the associated hydrodynamic forces which largely influenced the vertical bending moment.

4.1.4. Sagging and hogging moment peak value

Table 4 gives the percentage of error in the numerical calculation with nonlinear radiation force (fully nonlinear method) for the largest and second largest sagging peak during a complete test run. The largest percentage of error (24%) occurred for 3 Sisters wave case in 0.12 Froude number, however for rest of the cases, percentage of error was less than 20. The rule hogging and sagging moment for the containership calculated using Eq. (18) were respectively, 286 and 344 MN m, and the largest measured hogging and sagging peaks were 280 and 410MN.m, respectively. The rule bending moment was able to cover the largest hogging peak experienced by the ship in abnormal waves, but underestimated the largest sagging peak by 20%. However, several additional parameters needed to be considered in the rule bending moment before the final layout of the ship's hull is defined. Apart from that, other factors such as weather routing, the uncertainty associated with the measurements, additional safety factors associated with degradation due to corrosion etc. also needed to be taken into account before questioning the ability of the rule bending moment to ensure the structural safety of ships.

Figs. 11 and 12 present a comparison between results from the numerical codes and experimental data for the first and second largest hogging and sagging peaks. Each point in the horizontal axes corresponded to one wave condition. Use of body nonlinearity in the radiation/diffraction force had significantly improved the bending moment predictions compared to the partially nonlinear method. The newly estimated values were close to the experimental results. Similarly, hogging peak values were also improved, however, the amount of over estimation was higher than the sagging peak values

5. Conclusions

A body nonlinear time domain code based on strip theory was used to calculate the vertical responses of a container ship in extreme sea conditions including abnormal waves. The numerical code considered body nonlinearity in radiation/diffraction force along with body nonlinear Froude–Krylov and hydrostatic forces. Similarly, calculations were also made using a partially body nonlinear code that considered linear radiation/diffraction force with body nonlinear Froude–Krylov and hydrostatic force. The numerical results were compared with each other and also with the model tests experimental results.

Time series of the numerical and the experimental vertical motions were compared and the agreement was in general good. However, the ship tended to emerge more in the numerical simulations. The relative motion was underestimated by the numerical methods, which was probably due to the bow wave, dynamic swell up and the ship generated waves which were not taken into account in the numerical simulations.

The important conclusion from this study was related to the vertical bending moment prediction in extreme wave conditions: while the partial nonlinear time domain method largely overestimated the sagging peaks in extreme waves compared with model test results, inclusion of body nonlinearity in the radiation/diffraction forces significantly improved the sagging peak predictions in all the abnormal wave cases tested. In general, it was found that correct estimation of relative bow motion lead to accurate calculation of vertical bending moment at midship. The study emphasized that for ships with large bow flare and in extreme sea conditions, the body nonlinear hydrodynamic forces played a significant role on the load acting on them. Discrepancy was found during the comparison of hogging peaks between numerical and experimental results and the numerical hogging moments were found to be slightly over estimated.

Acknowledgements

This work was carried out within the European project "HANDLING WAVES - Decision Support System for Ship Operation in Rough Weather" (www.mar.ist.utl.pt/handlingwaves/), which was partly funded by the European Union through the Growth program under contract TST5-CT-2006-031489.

References

Buchner, B., 1995. The impact of green water on FPSO design. In: Proceedings of the Offshore Technology Conference. pp. 45–47.

Chan, K.K., Sclavonous, P.D., Jonkman, J., Hayman, J., 2015. Computation of nonlinear hydrodynamic loads on floating wind turbines using fluid-impulse theory. In: Proceedings of the 34th International Conference on Offshore Mechanics and Arctic Engineering, OMAE 2015-41053. St. John's, Newfoundland, Canada.

Clauss, G.F., Schmittner, C.E., 2005. Experimental optimization of extreme wave sequences for the deterministic analysis of wave/structure interaction. In: Proceedings of the ASME 2005 24th International Conference on Offshore Mechanics and Arctic Engineering. OMAE 2005-67049.

Clauss, G.F., Kauffeldt, A., Klein, M., 2009. Systematic investigation of loads and motions of a bulk carrier in extreme seas. In: Proceeding of the ASME 2009 28th International Conference on Ocean, Offshore and Arctic Engineering. OMAE 2009-79389.

Clauss, G.F., Klein, M., Dudek, M., 2010. Influence of the bow shape on loads in high and steep waves. In: Proceedings of the ASME 2010 29th International Conference on Ocean, Offshore and Arctic Engineering. OMAE2010-20142.

Cummins, W.E., 1962. The Impulse Response Function and Ship Motions. Schiffstechnik, 9, pp. 101–109. (Reprinted as David Taylor Model Basin Report).

Fonseca, N., Guedes Soares, C., 1998. Time-domain analysis of large-amplitude vertical ship motions and wave loads. J. Ship Res. 42 (2), 139–153.

Guedes Soares, C., Cherneva, Z., Antão, E.M., 2003. Characteristics of abnormal waves in North Sea storm sea states. Appl. Ocean Res. 25 (6), 337–344.

Guedes Soares, C., Fonseca, N., Pascoal, R., Clauss, G.F., Schmittner, C.E., Hennig, J.,

2006. Analysis of design wave loads on a FPSO accounting for abnormal waves. J. Offshore Mech. Arct. Eng. 128 (3), 241–247.
Guedes Soares, C., Fonseca, N., Pascoal, R., 2008. Abnormal wave induced load effects in ship structures. J. Ship Res. 52 (1), 30–44.
Kim, Y., Kim, K.H., Kim, J.H., Kim, T., Seo, M.G., Kim, Y., 2011. Time domain analysis of nonlinear motion responses and structural loads on ships and offshore structures: development of WISH programs. Int. J. Nav. Archit. Ocean Eng. 3, 37–52.
Kring, D., Huang, Y., Scalavounos, P., Vada, T., Braathen, A., 1997. Nonlinear ship motions and wave induced loads by a rankine method.In: Proceedings of the 21st Symp Naval Hydro. pp. 45–63.
Lin, W.M., Bergquist, J.R., Collette, M.D., Liut, D., Treakle, T.W., Weems, K.M., Weems, M.H.C., Zhang, S., 2008. Large Amplitude Motion Program (LAMP) for Ship Motions and Wave Loads Predictions Version 3.2.1. Tech. rept Science Applications International Corporation.
Mikami, T., Shimada, K., 2006. Time-domain strip method with memory-effect function considering the body nonlinearlity of ships in large waves. J. of Marine Science and Technology 11 (3), 139–149.
Ogilvie, T., 1964. Recent Progress towards the understanding and prediction of ship motions. In: Proceedings of the 6th Symposium on Naval Hydrodynamics.
Rajendran, S., Fonseca, N., Guedes Soares, C., 2011. Time domain comparison with experiments for ship motions and structural loads on a container ship in abnormal waves. In: Proceedings of the ASME 30th International Conference on Offshore Mechanics and Arctic Engineering, OMAE 2011, June 19–24. Rotterdam, the Netherlands.
Rajendran, S., Fonseca, N., Guedes Soares, C., 2012. Experiment and time domain method comparison for the responses of a container ship induced by the three Sisters abnormal waves. In: Guedes Soares, C., et al. (Eds.), Marine Technology and Engineering. Taylor & Francis, UK, pp. 223–230.
Rajendran, S., Fonseca, N., Guedes Soares, C., 2013. Estimation of short term probability distributions of wave induced loads acting on a cruise vessel in extreme seas. In: Proceedings of the 32nd International Conference on Offshore Mechanics and Arctic Engineering, OMAE 2013-11638.
Rajendran, S., Fonseca, N., Guedes Soares, C., 2015a. Simplified body nonlinear time domain calculation of vertical ship motions and wave loads in large amplitude waves. Ocean Eng. 107, 157–177.
Rajendran, S., Fonseca, N., Guedes Soares, C., 2015b. Effect of surge motion on the vertical response of ship in waves. Ocean Eng. 96, 125–138.
Salvesen, N., Tuck, E.O., Faltinsen, O., 1970. Ship motions and sea loads. Trans. SNAME 78, 250–287.
Wu, M.K., Moan, T., 1996. Linear and nonlinear hydroelastic analysis of high-speed vessels. J. Ship Res. 40 (2), 149–163.
Xia, J., Wang, Z., Jensen, J.J., 1998. Nonlinear wave loads and ship responses by a time-domain strip theory. Marine Struct. 11, 101–123.